

# Model predictive control of NPC three-level grid-tied converter based on reconstructed current

YANYAN LI<sup>1</sup>, HAN XIAO<sup>1</sup>, NAN JIN<sup>1</sup>, GUANGLU YAN<sup>1,2</sup> ✉

<sup>1</sup>College of Electrical and Information Engineering, Zhengzhou University of Light Industry  
China

<sup>2</sup>Nanyang Cigarette Factory, China Tobacco Henan Industrial Co., Ltd.  
China

e-mail: yangguanglu0@163.com

(Received: 28.07.2021, revised: 19.11.2021)

**Abstract:** The neutral point clamped (NPC) three-level grid-tied converter is the key equipment connecting renewable energy and power grids. The current sensor fault caused by harsh environment may lead to the split of renewable energy. The existing sensor fault-tolerant methods will reduce the modulation ratio index of the converter system. To ensure continuous operation of the converter system and improve the modulation index, a model predictive control method based on reconstructed current is proposed in this paper. According to the relationship between fault phase current and a voltage vector, the original voltage vector is combined and classified. To maintain the stable operation of the converter and improve the utilization rate of DC voltage, two kinds of fault phase current are reconstructed with DC current, normal phase current and predicted current, respectively. Based on reconstructed three-phase current, a current predictive control model is designed, and a model predictive control method is proposed. The proposed method selects the optimal voltage vector with the cost function and reduces time delay with the current reconstruction sector. The simulation and experimental results show that the proposed strategy can keep the NPC converter running stably with one AC sensor, and the modulation index is increased from 57.7% to 100%.

**Key words:** current reconstruction, current sensor fault, fault-tolerant, model predictive control, neutral point clamped three-level converter

## 1. Introduction

As the key connection equipment of a large capacity and high-power converter system, the reliability of the neutral point clamped (NPC) three-level grid-connected converter has always been concerned [1, 2]. However, current sensors may fail in harsh working conditions. There



© 2022. The Author(s). This is an open-access article distributed under the terms of the Creative Commons Attribution-NonCommercial-NoDerivatives License (CC BY-NC-ND 4.0, <https://creativecommons.org/licenses/by-nc-nd/4.0/>), which permits use, distribution, and reproduction in any medium, provided that the Article is properly cited, the use is non-commercial, and no modifications or adaptations are made.

are many factors that can cause sensor failures, such as board diagnostics socket terminal poor contact, a short circuit of nitrogen-oxygen sensor wiring harness, instrument underlying software error, crystallization at the inlet of postprocessors.

Converters are usually connected to an outdoor DC source, working under high pressure, high temperature, and humid conditions. In such a harsh environment, the current sensor may fall off or completely fail because its own magnetic components are made of fragile ferrite [3–5]. Therefore, it is urgent and important to study the fault-tolerant operation of converter systems.

Model predictive control (MPC) is widely used in nonlinear control because of its simple control and high reliability [6–9]. MPC needs first to establish a model of the control object, and then predict the next operation state based on the output and controllable input variables of the model, and select the optimal operation state through the cost function. However, when the current sensor fails, the MPC control strategy will fail due to the lack of feedback information, and the grid-tied converter will be paralyzed.

Thus, fault-tolerant sensors have been studied [10–17]. A sliding mode observer with adaptive regulation law was proposed to solve the problem that some sensor fault reconstruction methods need the upper bound of faults [10]. A vector space decomposition-based current estimation method was proposed to achieve fault-tolerant control over the current-sensor fault, and the voltage compensation based on that fault-tolerant control was presented for both open-phase and open-switch faults in [11]. A fault-estimation-based tolerant control strategy for a single-phase two-level pulse-width modulation rectifier subjected to a catenary current sensor fault and dc-link voltage sensor fault was proposed in [12]. An improved model of predictive power control based on reconstructed currents was proposed for the fault-tolerant operation of a grid-tied converter [13]. A proportional integral observer with unknown inputs was conceived in order to estimate states and sensor faults simultaneously. The stability of the system with the proposed fault-tolerant control strategy was formulated using the Lyapunov theory and the observer gains are obtained by solving linear matrices inequalities [14]. The differential algebraic-based fault diagnose method and adaptive fault-tolerant control strategy were presented [15]. Fault detection, localization, and tolerant control schemes of current sensors were presented for high-fault-tolerance induction motor drives [16].

In addition, an adaptive MPC method combining sensor fault tolerance with virtual synchronous machines was proposed [18]. For discrete-time systems, a fault-tolerant method was proposed, in which the normal state was recorded in real time and acted on the fault state [19]. A hybrid model for discrete-time systems with normal and fault states was established [20]. By combining the sliding mode observer with MPC, a sensor fault tolerance method for wind turbines was proposed [21]. A fault observer was developed to predict the fault information, and the min-imax MPC was used for fault tolerance [22]. Moreover, the Lyapunov stability theory and linear matrix inequality are used to form a closed-loop system to realize fault-tolerant control [23].

The above fault-tolerant methods of the current sensor need to design complex observers or fault-tolerant models, because the available information after faults is insufficiently utilized. At present, the research on the current sensor fault of the NPC three-level grid-connected converter has not been deepened. For the NPC three-level grid-tied converter with current sensor faults, a model predictive fault-tolerant control method based on current reconstruction is proposed in this paper. When the current sensor fails, the relationship between the voltage vector and current is analyzed. The voltage vector is divided into the voltage vector that can directly reconstruct fault

phase current, the voltage vector that can reconstruct fault phase current by predicting current and other voltage vectors. The voltage vector combination is formed by the voltage vector, which can reconstruct fault phase current. Under the voltage vector combination, fault phase current is calculated by predicted current or DC current and normal phase current. Then, the current reconstruction sector is used to reduce the converter system delay. Simulations and experiments verify the effectiveness of the control strategy. The proposed MPC method based on current reconfiguration is applied to the fault-tolerant control of the NPC three-level grid-tied converter, and the reliability of the power grid is improved.

## 2. Current reconstruction and predictive control model

### 2.1. Current reconstruction model

To avoid the impact of AC current sensor faults on the power grid, a current sensor is added to the DC side for fault-tolerant control. The normal phase AC current sensor collects the normal phase current and feeds the collected signal back to the control module.

As shown in Fig. 1, the topology of the NPC three-level grid-tied converter contains twelve insulated gate bipolar transistors (IGBTs) and the DC power  $U_{dc}$ . The three-phase load is connected to filtering the inductor  $L$  and parasitic resistor  $R$ . The three-phase currents of the DC voltage source are represented by  $i_a, i_b$  and  $i_c$ ;  $e_a, e_b, e_c$  represent the grid voltage. The currents of phase  $a$  and  $b$  are sampled by the current sensor. The current of can be obtained as  $-i_a -i_b$ . However, if the phase  $b$  current sensor (taking phase  $b$  as an example) fails, the current of phase  $b$  and phase  $c$  cannot be obtained, resulting in the converter control failure.

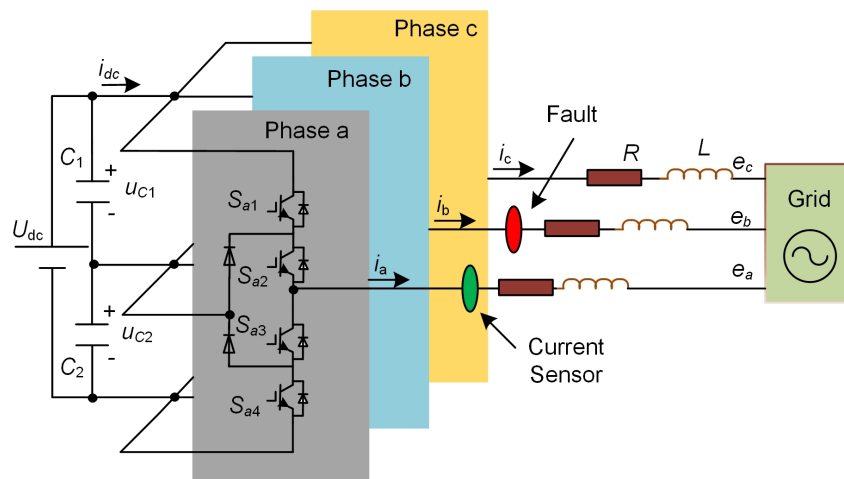


Fig. 1. Topology of NPC three-level grid-tied converter with current sensor fault in phase  $b$

The relationship between the DC current  $i_{dc}$  and the switching state of each bridge arm is:

$$i_{dc} = S_{ua} \times i_a + S_{ub} \times i_b + S_{uc} \times i_c, \tag{1}$$

where  $S_{ua}$ ,  $S_{ub}$ , and  $S_{uc}$  represent the switching state and are defined as:

$$S_{ux} = \begin{cases} 1 & S_x = 0 \\ 0 & \text{others} \end{cases}, \quad x = a, b, c. \quad (2)$$

Then, when the phase  $b$  current sensor fails, the expression of  $i_b$  and  $i_c$  can be deduced.

$$\begin{cases} (S_{ub} - S_{uc})i_b = i_{dc} - (S_{ua} - S_{uc})i_a \\ (S_{uc} - S_{ub})i_c = i_{dc} - (S_{ua} - S_{ub})i_a \end{cases}. \quad (3)$$

Based on (3), when  $S_{uc} \neq S_{ub}$ , the phase  $b$  current  $i_b$  or phase  $c$  current  $i_c$  can be reconstructed by DC current  $i_{dc}$  and phase  $a$  current  $i_a$ . Then the voltage vectors which can be used are  $U5(1, 1, 0)$ ,  $U7(0, 1, 0)$ ,  $U11(0, 0, 1)$ ,  $U13(1, 0, 1)$ ,  $U16(0, 1, -1)$ ,  $U17(-1, 1, 0)$ ,  $U18(-1, 0, 1)$ ,  $U19(0, -1, 1)$ ,  $U22(1, 1, -1)$ ,  $U23(-1, 1, -1)$ ,  $U25(-1, -1, 1)$  and  $U26(1, -1, 1)$ , as shown in Fig. 2.

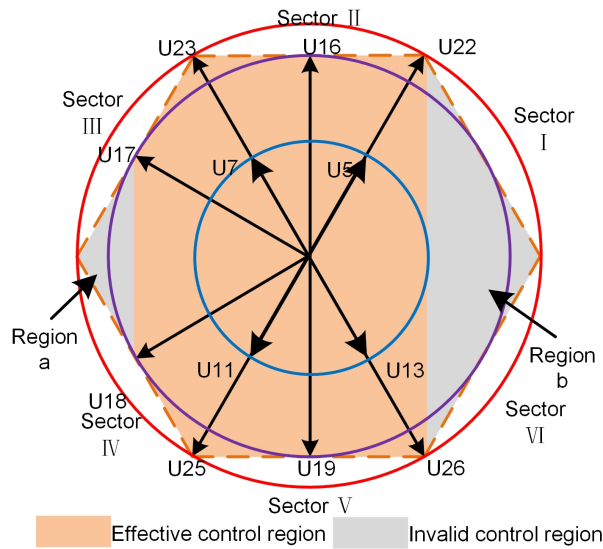


Fig. 2. Combination based on 12 voltage vectors current reconstruction

For 12 voltage vectors that can be directly used for current reconstruction, the DC current  $i_{dc}$  is related to the AC current  $i_b$ , thus the normal DC current  $i_{dc}$  and the phase  $a$  current  $i_a$  can be used to obtain the three-phase current. As shown in Table 1, the current relationship is established with (3). The three-phase current is obtained by current reconstruction method to improve the reliability of current sensor fault operation. When the converter output voltage reaches a certain limit, the DC voltage is insufficient to output the converter output voltage amplitude, and modulation index is 57.7%.

When AC current cannot be reconstructed directly from Table 1 or (3), the phase  $b$  current  $i_b$  is reconstructed with the prediction current  $i_b(k + 1)$ .

Table 1. Current relationship and reconstructed current under 12 voltage vectors

Voltage vector	DC current $i_{dc}$	Phase $a$ current $i_{ar}$	Phase $b$ current $i_{br}$	Phase $c$ current $i_{cr}$
$U5(1, 1, 0)$	$i_{dc}$	$i_a$	$i_{dc} - i_{ar}$	$-i_{ar} - i_{br}$
$U7(0, 1, 0)$	$i_{dc}$	$i_a$	$i_{dc}$	$-i_{ar} - i_{br}$
$U11(0, 0, 1)$	$i_{dc}$	$i_a$	$-i_{dc} - i_{ar}$	$-i_{ar} - i_{br}$
$U13(1, 0, 1)$	$i_{dc}$	$i_a$	$-i_{dc}$	$-i_{ar} - i_{br}$
$U16(0, 1, -1)$	$i_{dc}$	$i_a$	$i_{dc}$	$-i_{ar} - i_{br}$
$U17(-1, 1, 0)$	$i_{dc}$	$i_a$	$i_{dc}$	$i_{ar} - i_{br}$
$U18(-1, 0, 1)$	$i_{dc}$	$i_a$	$i_{dc} - i_{ar}$	$-i_{ar} - i_{br}$
$U19(0, -1, 1)$	$i_{dc}$	$i_a$	$-i_{dc} - i_{ar}$	$-i_{ar} - i_{br}$
$U22(1, 1, -1)$	$i_{dc}$	$i_a$	$i_{dc} - i_{ar}$	$-i_{ar} - i_{br}$
$U23(-1, 1, -1)$	$i_{dc}$	$i_a$	$i_{dc}$	$-i_{ar} - i_{br}$
$U25(-1, -1, 1)$	$i_{dc}$	$i_a$	$-i_{dc} - i_{ar}$	$-i_{ar} - i_{br}$
$U26(1, -1, 1)$	$i_{dc}$	$i_a$	$-i_{dc}$	$-i_{ar} - i_{br}$

The current reconstruction method includes one DC sensor and one AC current sensor to obtain three-phase current, which improves reliability and fault-tolerance.

## 2.2. Predictive control model

The current reconstruction is applied in case of current-sensor failure. MPC and the detailed model of current reconstruction are shown in this section.

The switching state of each phase  $S_i$  is defined as (4).

$$S_i = \begin{cases} 1 & S_{i1} = \text{on}, S_{i2} = \text{on}, S_{i3} = \text{off}, S_{i4} = \text{off} \\ 0 & S_{i1} = \text{on}, S_{i2} = \text{off}, S_{i3} = \text{off}, S_{i4} = \text{on} \\ -1 & S_{i1} = \text{off}, S_{i2} = \text{off}, S_{i3} = \text{on}, S_{i4} = \text{on} \end{cases}, \quad (4)$$

where:  $S_i$  ( $I \in \{a, b, c\}$ ) denotes the power switch in the main circuit, “on” and “off” represent the power switch turned on and turned off, respectively.

The NPC three-level grid-tied converter has 27 switching state combinations. Each switch state combination corresponds to an output voltage vector. The NPC three-level converter can generate 27 voltage vectors as shown in Fig. 3. The output voltage vector  $U_n$  can be expressed as (5).

$$U_n = \frac{2}{3} \left( u_a e^{j0} + u_b e^{j\frac{2\pi}{3}} + u_c e^{-j\frac{2\pi}{3}} \right), \quad n = 0, \dots, 26, \quad (5)$$

where:  $u_a, u_b, u_c$  represents the three-phase output voltage of the converter.

In addition, the three-phase output voltage can be expressed as (6).

$$u_a = \frac{1}{2} U_{dc} S_a, \quad u_b = \frac{1}{2} U_{dc} S_b, \quad u_c = \frac{1}{2} U_{dc} S_c. \quad (6)$$

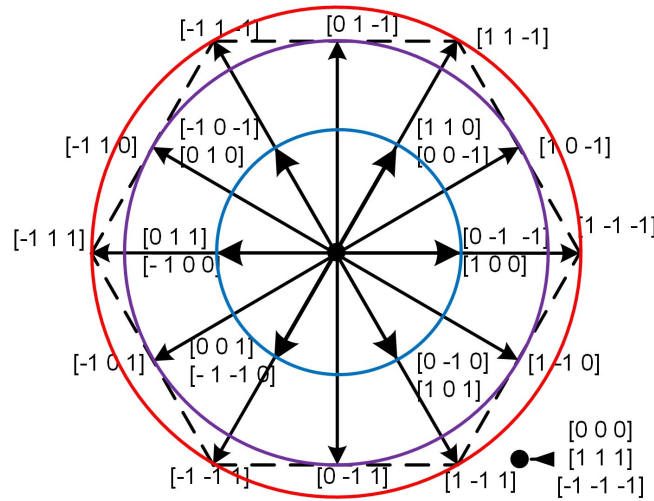


Fig. 3. Three-level voltage vector of conventional NPC

In the  $\alpha\beta$  coordinate system,  $u_\alpha, u_\beta$  can be expressed as (7).

$$\begin{bmatrix} u_\alpha \\ u_\beta \end{bmatrix} = \frac{2}{3} \begin{bmatrix} 1 & -1/2 & 1/2 \\ 0 & \sqrt{3}/2 & -\sqrt{3}/2 \end{bmatrix} \begin{bmatrix} u_a \\ u_b \\ u_c \end{bmatrix}, \quad (7)$$

where  $u_\alpha$  and  $u_\beta$  represent the output voltage of the NPC three-level converter.

The voltage equation based on the Kirchhoff's voltage law can be obtained as (8).

$$L \frac{di_{\alpha\beta}}{dt} = u_{\alpha\beta} - Ri_{\alpha\beta} - e_{\alpha\beta}, \quad (8)$$

where:  $\mathbf{u}_{\alpha\beta} = [u_\alpha(k), u_\beta(k)]^T$ ,  $u_\alpha$  and  $u_\beta$  represent the output voltages of the converter;  $\mathbf{i}_{\alpha\beta} = [i_\alpha(k), i_\beta(k)]^T$ ,  $i_\alpha$  and  $i_\beta$  are the represent output currents of the converter;  $\mathbf{e}_{\alpha\beta} = [e_\alpha(k), e_\beta(k)]^T$ ,  $e_\alpha$  and  $e_\beta$  represent the grid voltage.

After discretization using forward Euler discretization, (9) can be deduced:

$$L \frac{[i_{\alpha\beta}(k+1) - i_{\alpha\beta}(k)]}{T_s} = u_{\alpha\beta}(k) - Ri_{\alpha\beta}(k) - e_{\alpha\beta}(k), \quad (9)$$

where:  $T_s$  represents the sampling period;  $X(k)$  is the variable  $X$  at the  $k$ th instant, and  $X(k+1)$  stands for the variable  $X$  at the  $(k+1)$ th instant.

In order to obtain the predicted current at the  $(k+1)$ th instant, (10) can be deduced.

$$i_{\alpha\beta}(k+1) = \frac{L - RT_s}{L} i_{\alpha\beta}(k) + \frac{T_s}{L} [u_{\alpha\beta}(k) - e_{\alpha\beta}(k)]. \quad (10)$$

### 3. Current reconstruction based on sector selection

The conventional MPC voltage vector selection method is to calculate 27 voltage vectors and select the optimal vector. 27 calculations are needed in each cycle, and 18 calculations are needed when the current sensor fails. The increase of calculation time is usually accompanied by the increase of system delay. In order to reduce the calculation time, a voltage vector selection method based on a current reconstruction sector is proposed. Firstly, the grid-side voltage is used to select a current reconstruction sector, and then the optimal voltage vector is selected from the sector. In this way, only one current reconstruction sector selection and five vector selections are needed in each cycle, which reduces the calculation process by 12 times.

The 12 voltage vectors in Fig. 2 are unable to complete the control voltage vector, and the load current will be out of control when the DC voltage cannot meet the amplitude of the voltage vector. Thus, the current reconstruction sector and six predictive voltage vectors are adopted.

In Fig. 4, 27 voltage vectors are reduced to 18 voltage vectors, which control the NPC converter. According to Table 2 and (10), the combined 18 voltage vectors are additionally added with  $U3(1, 0, 0)$ ,  $U10(-1, 0, 0)$ ,  $U15(1, 0, -1)$ ,  $U20(1, -1, 0)$ ,  $U21(1, -1, -1)$ ,  $U24(-1, 1, 1)$ .

$$\begin{cases} X = \begin{cases} 1 & e_x > 0 \\ 0 & \text{others} \end{cases}, x = A, B, C \\ N = A + 2B + 4C \end{cases}, \quad (11)$$

where:  $U_x$  represent the voltage of the phase  $x$ , and  $X$  and  $N$  are the computational operators.

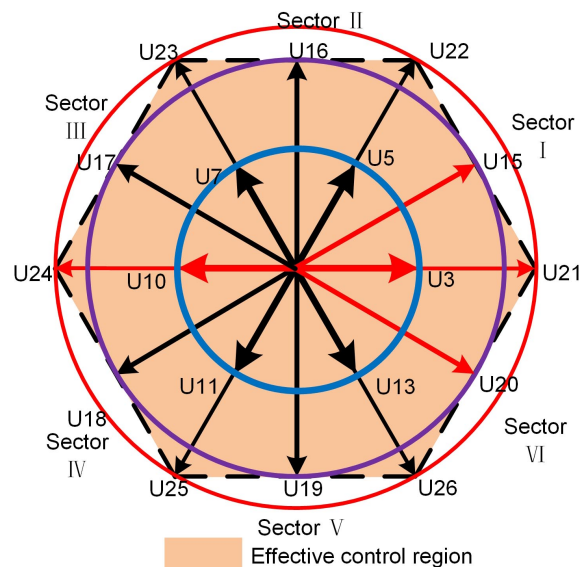


Fig. 4. Voltage vector with current sensor fault

The voltage vector directly used for current reconstruction and the voltage vector with prediction constitute the control vector set shown in Fig. 4. Under the voltage vector set, the load

Table 2. Sector's classification and voltage vectors to be predicted

Sector	I	II	III	IV	V	VI
$N$	3	1	5	4	6	2
Voltage vectors to be predicted	$U_3, U_{21}, U_{15}$	–	$U_{10}, U_{24}$	$U_{10}, U_{24}$	–	$U_3, U_{21}, U_{20}$

current will not be out of control in region  $a$  and region  $b$  and the modulation index is 100%. The adoption of current reconstruction sectors shortens the computation time, as shown in Table 2. Therefore, the voltage vector combination based on current reconstruction sector selection does not cause a lack of current control in region  $a$  and region  $b$ . In addition, the three-level 27 voltage vectors are divided into 3 types, as shown in Fig. 5.

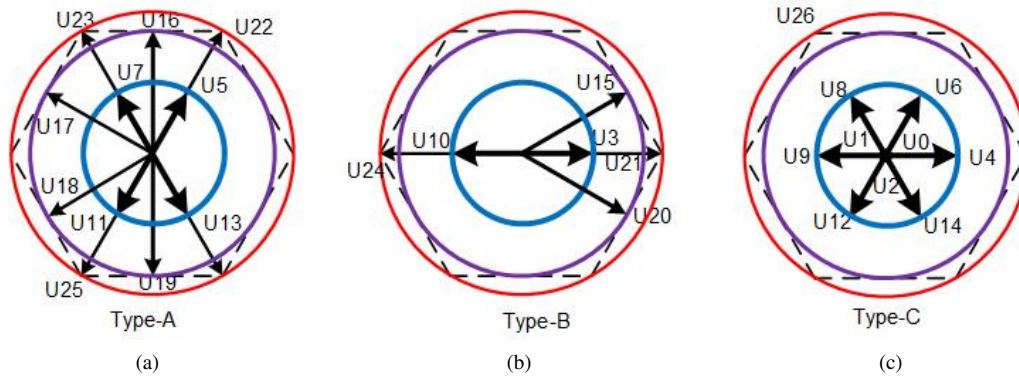


Fig. 5. Voltage vector classification based on current reconstruction: type-A voltage vector (a); type-B voltage vector (b); type-C voltage vector (c)

**Type-A:** The voltage vectors can be reconstructed directly by the DC current  $i_{dc}$  and phase  $a$  current  $i_a$ , including  $U_5(1, 1, 0)$ ,  $U_7(0, 1, 0)$ ,  $U_{11}(0, 0, 1)$ ,  $U_{13}(1, 0, 1)$ ,  $U_{16}(0, 1, -1)$ ,  $U_{17}(-1, 1, 0)$ ,  $U_{18}(-1, 0, 1)$ ,  $U_{19}(0, -1, 1)$ ,  $U_{22}(1, 1, -1)$ ,  $U_{23}(-1, 1, -1)$ ,  $U_{25}(-1, -1, 1)$  and  $U_{26}(1, -1, 1)$ .

**Type-B:** The voltage vectors of three-phase current can be reconstructed by the predictive current  $i_b(k+1)$ , including  $U_3(1, 0, 0)$ ,  $U_{10}(-1, 0, 0)$ ,  $U_{15}(1, 0, -1)$ ,  $U_{20}(1, -1, 0)$ ,  $U_{21}(1, -1, -1)$  and  $U_{24}(-1, 1, 1)$ .

**Type-C:** Zero vectors and voltage vectors that can be replaced by the same function, including  $U_0(0, 0, 0)$ ,  $U_1(1, 1, 1)$ ,  $U_2(-1, -1, -1)$ ,  $U_4(0, -1, -1)$ ,  $U_6(0, 0, -1)$ ,  $U_8(-1, 0, -1)$ ,  $U_9(0, 1, 1)$ ,  $U_{12}(-1, -1, 0)$  and  $U_{14}(0, -1, 0)$ .

MPC strategy takes a lot of time to calculate the optimal voltage vector, and there is a certain delay between the optimal vector and the practical vector. The proposed method is combined with current reconstruction sector selection, and the counter clockwise rotation of the current reconstruction sector shortens the calculation time. In addition, the proposed method also makes up for the problem of insufficient capacity when there are only 12 voltage vectors.

To simplify the program's running process, reorder the 18 voltage vectors of the combination, and the control structure shown in Fig. 6.

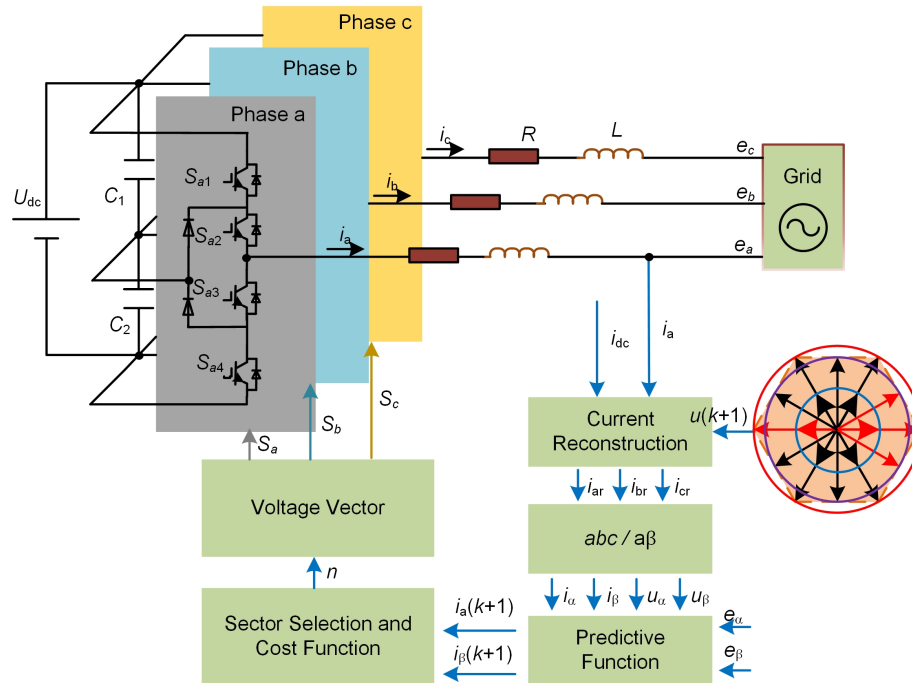


Fig. 6. The control structure of proposed method with reconstructed current and sector selection

The simplified vector selection process is as follows:

- Step 1: Collect the grid side voltage  $e(k)$ , phase  $a$  current  $i_a(k)$  and DC current  $i_{dc}(k)$ .
- Step 2: Calculate  $N$  with (12) and select the current reconstruction sector  $y$ .
- Step 3: Select the optimal voltage vector  $U_j$  in the current reconstruction sector.
- Step 4: Current reconstruction  $i_b(k)$  or (1) according to  $U_j$ .
- Step 5: Reconstruct  $i_c(k)$  with (10).

The voltage vector that can minimize the cost function is defined as the optimal voltage vector and is used in the control of the converter at the next instant. Considering the neutral point current, the cost function is defined as the sum of the absolute error between the reference current and the predicted current plus the difference of DC capacitor voltage:

$$g = |i_{a\text{ref}} - i_\alpha(k + 1)| + |i_{\beta\text{ref}} - i_\beta(k + 1)| + p|u_{c1} - u_{c2}|, \quad (12)$$

where:  $i_{a\text{ref}}$  and  $i_{\beta\text{ref}}$  represent the reference current,  $u_{c1}$  and  $u_{c2}$  are the voltages of the upper and lower capacitors,  $p$  is the weight factor of voltage balance.

The predicted currents of different voltage vectors at the next instant are obtained with (10) and the prediction function. In order to obtain the ideal predicted current, the optimal voltage vector is determined by using the cost function, (12), through the improved voltage vector selection

method. The voltage vector which minimizes the cost function  $g$  is used as the best choice for the NPC converter.

The fault of the AC current sensor reduces the reliability of the NPC converter. When the phase  $b$  current sensor fails, the three-phase current is reconstructed with the current relationship under different voltage vectors in Table 1. Then the reconstructed current  $i_{abc}$  is directly involved in the circuit when the current sensor fails.

#### 4. Simulation and experimental verification

To further verify the proposed MPC strategy based on current reconstruction, the hardware-in-the-loop experimental platform shown in Fig. 7 is built. The hardware in the loop experimental platform uses PXIe-1071 of the TI company as a hardware circuit and controller. The test instrument is a Yokogawa DLM4000 series oscilloscope, and experimental parameters are shown in Table 3.

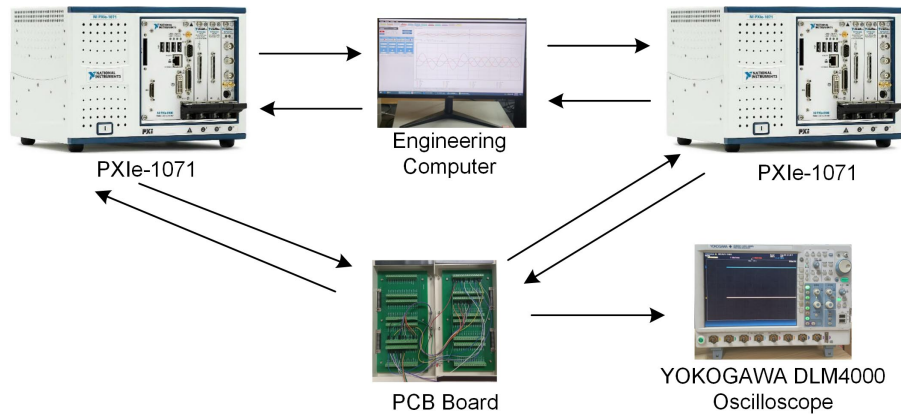


Fig. 7. Hardware in the loop experimental platform

Table 3. Simulation and experimental parameters

Symbol	Parameters	Values
$U_{dc}$	DC voltage	400 V
$e$	RMS of grid phase voltage	110 V
$L$	Filter inductance	0.01 H
$R$	Parasitic resistance	0.05 $\Omega$
$f_s$	Sampling frequency	10 kHz
$f$	Grid frequency	50 Hz
$C_1, C_2$	Capacitance	4700 $\mu\text{F}$

#### 4.1. Comparison of voltage vector selection

Method-A: only using 12 type-A voltage vectors.

Method-B: using 12 type-A voltage vectors and 6 type-B voltage vectors. Their effects are compared in Fig. 8.

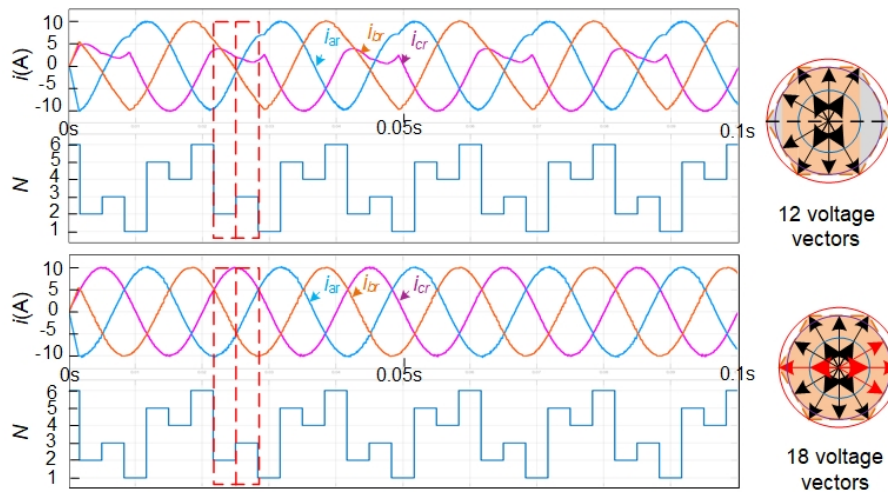


Fig. 8. Comparison of voltage vector selection methods

When the DC voltage  $U_{dc} = 400$  V, the three-phase currents reconstructed by method-A has obvious collapse at  $N = 2$  and  $N = 3$ , while the three-phase current waveform reconstructed by method-b can control the current waveform in region-a and region-b. This is because when the voltage vector does not reach the amplitude of the reference voltage vector in the actual operation process, the method-A cannot control the current and causes the current to decrease and a modulation index is 57.7%. Method-A has no appropriate voltage vector control in region-a and region-b, while method-B can use voltage vector control in the whole hexagon region and a modulation index is 100%.

#### 4.2. Steady state experimental

The steady-state control performance of the proposed method is tested and compared with the normal state NPC three-level grid-connected conversion effect. Figure 9(a) shows the current waveform results before the phase  $b$  current sensor fault when the reference current is 10 A. Figure 9(b) shows the current waveform results after the phase  $b$  current sensor fault when the reference current is 10 A.

In Fig. 9, when the reference current is 10 A, the total harmonic distortion of the current in the normal state is 3.32%, while the total harmonic distortion of the proposed current reconstruction strategy is 4.16%, and the errors of the two currents are not more than 1 A. There is a certain mathematical relationship between DC current and AC current under each voltage vector, thus, the DC current can replace the current sensor for current reconstruction.

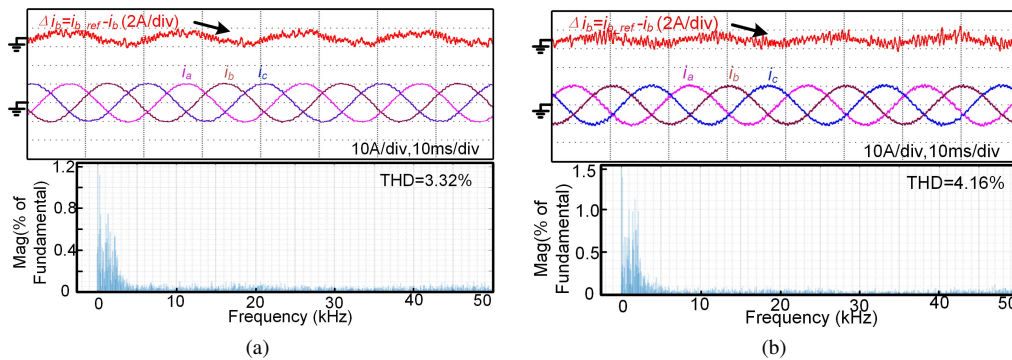


Fig. 9. Comparison before and after current reconstruction when the reference current is 10 A: three phase current before current sensor b fault (a); three phase current after current sensor b fault (b)

### 4.3. Dynamic state simulation

The dynamic performance of the proposed method is tested. Figure 10 shows the dynamic process of the reconstructed current when the reference current decreases from 15 A to 10 A. Figure 11 shows the dynamic process of the reconstructed current when the reference current increases from 10 A to 15 A. Figure 12 shows the dynamic process from pre-fault to current reconstruction of the current sensor.

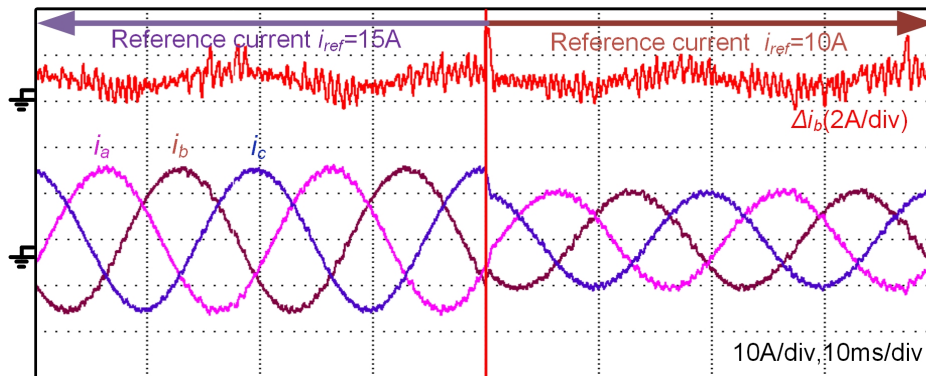


Fig. 10. Three phase dynamic current reduces from 15 A to 10 A

When the current sensor fails, the three-phase current has obvious distortion, and the proposed method can quickly adjust the converter to the normal operation state by using the MPC based on current reconstruction. When the reference current is transformed, the proposed current reconstruction method can keep up with the reference current, and the current error remains within 1 A. The effectiveness of the proposed method is further verified and the fault tolerance performance of the NPC grid-tied converter is improved.

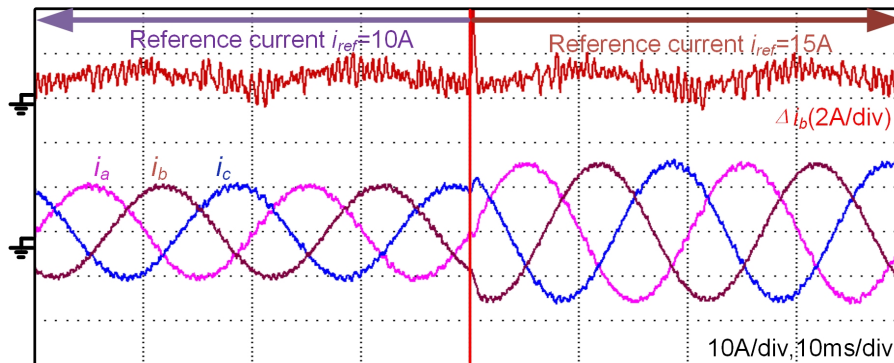


Fig. 11. Three phase dynamic current increases from 10 A to 15 A

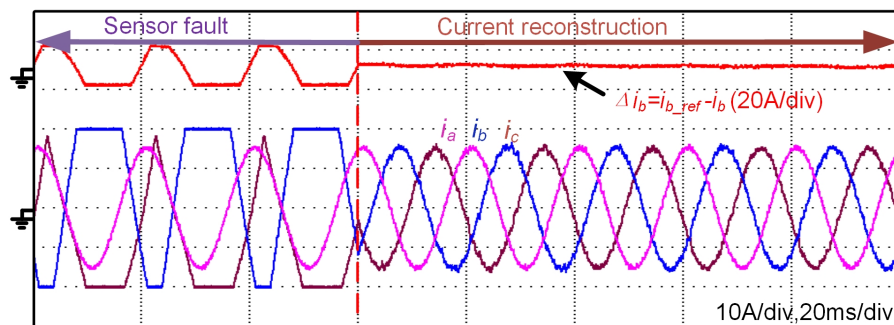


Fig. 12. Comparison before and after current reconstruction when the reference current is 15 A

## 5. Conclusion

The controller of the NPC three-level grid-tied converter needs the grid side current signal. Once the current sensor fails, the current generated by the converter will have a great impact on the grid. To solve this problem, an MPC strategy based on current reconstruction is proposed.

1. When the current sensor fails, the three-phase current is reconstructed by using the relationship between the voltage vector and current. The reconstructed three-phase current participates in MPC to maintain the fault-tolerant operation of the converter.
2. When the current sensor fails, the type-A voltage vector is used to replace the original voltage vector for MPC. This method can realize the fault tolerant operation of converters after faults of the current sensor.
3. The proposed method-A cannot normally control the current in region-a and region-b, that is, the modulation index is low. On the basis of method-A, adding a type-B voltage vector and selecting a current reconstruction sector can improve a modulation index and reduce the calculation delay of MPC.

4. Experimental results show that when the current sensor fails, the proposed method-B can adjust the reconstructed current with a voltage vector. The control strategy enhances the continuous operation ability of the power grid.

#### Acknowledgements

The authors gratefully acknowledge the National Nature Science Foundation of China under Grant U2004166, the Scientific and Technological Project in Henan Province under Grant 212102210021, the Youth Talent Support Project of Henan Province under Grant 2019HYTP021, and Science and Technology Innovation Team in Universities of Henan Province under Grant 22IRTSTHN017.

#### References

- [1] Erdiwansyah M., H Husin., Nasaruddin., *A critical review of the integration of renewable energy sources with various technologies*, Protection and Control of Modern Power Systems, vol. 6, no. 1, pp. 3945–3948 (2021), DOI: [10.1186/s41601-021-00181-3](https://doi.org/10.1186/s41601-021-00181-3).
- [2] Kaniewski J.Z., *Power flow controller based on bipolar direct PWM AC/AC converter operation with active load*, Archives of Electrical Engineering, vol. 68, no. 2, pp. 341–356 (2019), DOI: [10.24425/ae.2019.128272](https://doi.org/10.24425/ae.2019.128272).
- [3] Bouakoura M. et al., *Novel speed and current sensor FDI schemes with an improved AFTC for induction motor drives*, Advances in Electrical and Electronic Engineering, vol. 16, no. 1, pp. 1–14 (2018), DOI: [10.15598/aece.v16i1.2573](https://doi.org/10.15598/aece.v16i1.2573).
- [4] Adamczyk M., Orłowska-Kowalska T., *Virtual current sensor in the fault-tolerant field-oriented control structure of an induction motor drive*, Sensors, vol. 19, no. 22 (2019), DOI: [10.3390/s19224979](https://doi.org/10.3390/s19224979).
- [5] Wang X.Q., Wang Z., Xu Z.X., *Comprehensive diagnosis and tolerance strategies for electrical faults and sensor faults in dual three-phase PMSM drives*, IEEE Transactions on Power Electronics, vol. 34, no. 7, pp. 6669–6684 (2019), DOI: [10.1109/TPEL.2018.2876400](https://doi.org/10.1109/TPEL.2018.2876400).
- [6] Nebeluk R., Marusak P., *Efficient MPC algorithms with variable trajectories of parameters weighting predicted control errors*, Archives of Control Sciences, vol. 30, no. 2, pp. 325–363 (2020), DOI: [10.24425/acs.2020.133502](https://doi.org/10.24425/acs.2020.133502).
- [7] Li Y., Diao F., Zhao Y., *Simplified two-stage model predictive control for a hybrid multilevel converter with floating h-bridge*, IEEE Transactions on Power Electronics, vol. 36, no. 4, pp. 4839–4850 (2021), DOI: [10.1109/TPEL.2020.3018956](https://doi.org/10.1109/TPEL.2020.3018956).
- [8] Falkowski P., Sikorski A., Kulikowski K. et al., *Model predictive control of power converters for robust and fast operation of AC microgrids*, Bulletin of the Polish Academy of Sciences: Technical Sciences, vol. 68, no. 1, pp. 51–60 (2020), DOI: [10.24425/bpasts.2020.131836](https://doi.org/10.24425/bpasts.2020.131836).
- [9] Teng Q., Xu R., Han X., *Properties of active rectifier with LCL filter in the selection process of the weighting factors in finite control set-MPC*, IEEE Transactions on Energy Conversion, vol. 35, no. 4, pp. 2249–2260 (2020), DOI: [10.1109/TEC.2020.3015984](https://doi.org/10.1109/TEC.2020.3015984).
- [10] Zhang Z.L., Xiao B.X., *Sensor fault diagnosis and fault tolerant control for forklift based on sliding mode theory*, IEEE Access, vol. 8, pp. 84858–84866 (2020), DOI: [10.1109/ACCESS.2020.2991188](https://doi.org/10.1109/ACCESS.2020.2991188).
- [11] Wang X.Q., Wang Z., Xu Z.X., *Comprehensive Diagnosis and tolerance strategies for electrical faults and sensor faults in dual three-phase PMSM drives*, IEEE Transactions on Power Electronics, vol. 34, no. 7, pp. 6669–6684 (2019), DOI: [10.1109/TPEL.2018.2876400](https://doi.org/10.1109/TPEL.2018.2876400).
- [12] Gong Z.F., Huang D.Q., Jadoon H.U.K., *Sensor-fault-estimation-based tolerant control for single-phase two-level PWM rectifier in electric traction system*, IEEE Transactions on Power Electronics, vol. 35, no. 11, pp. 12274–12284 (2020), DOI: [10.1109/TPEL.2020.2982689](https://doi.org/10.1109/TPEL.2020.2982689).

- [13] Yao G., Li Y.Y., Li Q., *Model predictive power control for a fault-tolerant grid-tied converter using reconstructed currents*, IET Power Electronics, vol. 13, no. 6, pp. 1181–1190 (2020), DOI: [10.1049/iet-pel.2019.0465](https://doi.org/10.1049/iet-pel.2019.0465).
- [14] Jamel W., Khedher A., Ben O.K., *Observer design and active fault tolerant control for Takagi-Sugeno systems affected by sensors faults*, International Journal of Modelling, Identification and Control, vol. 27, no. 1, pp. 22–30 (2017), DOI: [10.1504/IJMIC.2017.10003318](https://doi.org/10.1504/IJMIC.2017.10003318).
- [15] Li H.M., Yao H.Y., Hou S.H., *Current sensor fault diagnosis and adaptive fault-tolerant control of PMSM drive system based on differential algebraic method*, International Journal of Applied Electromagnetics and Mechanics, vol. 53, no. 3, pp. 551–565 (2017), DOI: [10.3233/JAE-160090](https://doi.org/10.3233/JAE-160090).
- [16] Yu Y., Zhao Y.Z., Wang B., *Current sensor fault diagnosis and tolerant control for VSI-based induction motor drives*, IEEE Transactions on Power Electronics, vol. 33, no. 5, pp. 4238–4248 (2018), DOI: [10.1109/TPEL.2017.2713482](https://doi.org/10.1109/TPEL.2017.2713482).
- [17] Soukaina E.D., Loubna L., Mustapha A.L., *Sliding mode approach applied to sensorless direct torque control of cage asynchronous motor via multi-level inverter*, Protection and Control of Modern Power Systems, vol. 5, no. 1 (2020), DOI: [10.1186/s41601-020-00159-7](https://doi.org/10.1186/s41601-020-00159-7).
- [18] Jin N., Pan C., Li Y.Y., *Model predictive control for virtual synchronous generator with improved vector selection and reconstructed current*, Energies, vol. 13, no. 20 (2020), DOI: [10.3390/en13205435](https://doi.org/10.3390/en13205435).
- [19] Li J., Zhang D.F., Wang Z.Q., *Novel MPC-based fault tolerant tracking control against sensor faults*, Asian Journal of Control, vol. 22, no. 2, pp. 841–854 (2020), DOI: [10.1002/asjc.1966](https://doi.org/10.1002/asjc.1966).
- [20] Zhang H., Liang J., Zhang Z.Y., *Active fault tolerant control of adaptive cruise control system considering vehicle-borne millimeter wave radar sensor failure*, IEEE Access, vol. 8, pp. 11228–11240 (2020), DOI: [10.1109/ACCESS.2020.2964947](https://doi.org/10.1109/ACCESS.2020.2964947).
- [21] Ghanbarpour K., Bayat F., Jalilvand A., *Wind turbines sustainable power generation subject to sensor faults: observer-based MPC approach*, International Transactions on Electrical Energy Systems, vol. 30, no. 1 (2019), DOI: [10.1002/2050-7038.12174](https://doi.org/10.1002/2050-7038.12174).
- [22] Huang C., Naghdy F., Du H.P., *Observer-based fault-tolerant controller for uncertain steer-by-wire systems using the delta operator*, IEEE-ASME Transactions on Mechatronics, vol. 23, no. 6, pp. 2587–2598 (2018), DOI: [10.1109/TMECH.2018.2820091](https://doi.org/10.1109/TMECH.2018.2820091).
- [23] Zheng Y., Liu Z.L., Liu L.Y., *Robust MPC-based fault-tolerant control for trajectory tracking of surface vessel*, IEEE Access, vol. 6, pp. 14755–14763 (2018), DOI: [10.1109/ACCESS.2018.2817345](https://doi.org/10.1109/ACCESS.2018.2817345).